Earth Systems and Environment
https://doi.org/10.1007/s41748-025-00868-9

ORIGINAL ARTICLE

Machine Learning-Driven Mapping of Heatwave Health Risks Across Local Climate Zones in a Mediterranean Context

Dyna Chourouk Zitouni[1,2,3] · Djihed Berkouk[2,4] · Mohamed Elhadi Matallah[2,3,5] · Mohamed Akram Eddine Ben Ratmia[2] · Ayyoob Sharifi[6] · Shady Attia[3]

Received: 9 August 2025 / Revised: 23 September 2025 / Accepted: 26 September 2025

Abstract

Mediterranean cities are increasingly vulnerable to extreme heat events, driven by rapid urbanization and climate change. This study proposes a high-resolution framework for assessing heat-health risk (HHR) in Algiers, Algeria, by integrating the Heat Health Risk Index (HHRI) and Surface Urban Heat Island (SUHI) metrics within the Local Climate Zone (LCZ) classification 2020 system. Drawing on multi-temporal satellite data (2015–2023), demographic information, and meteorological records, we generated hazard, exposure, and vulnerability layers, with variable weighting derived from Principal Component Analysis (PCA). SUHI was estimated using Landsat-based Land Surface Temperature (LST) data, referencing rural LCZs as thermal baselines. Unsupervised K-means clustering was employed to classify combined HHRI–SUHI data, revealing four distinct urban heat risk profiles. The results indicate that LCZs 4, 5, and 8 are most affected by compounded heat-health risks, while LCZs 4, 6, and 8 display the highest surface heat accumulation. The resulting typologies identify zones where thermal stress intersects with social vulnerability, offering valuable insights for targeted adaptation. This is the first study in North Africa and the Mediterranean to apply this integrated clustering approach, demonstrating its applicability to other heat-prone, data-scarce urban environments.

Graphical Abstract

This graphical abstract illustrates an integrated geospatial and machine learning framework developed to assess urban heat-health risk in Algiers, Algeria a densely populated Mediterranean city facing rising exposure to extreme heat events. The study combines multi-year satellite-derived Land Surface Temperature (LST), demographic indicators, and meteorological data from 2015 to 2023. Using the Local Climate Zone (LCZ) classification, the urban landscape was stratified based on morphological and thermal characteristics. The Heat Health Risk Index (HHRI) was computed through a hazard–exposure–vulnerability framework, with variable weighting based on Principal Component Analysis (PCA). In parallel, SUHI intensity was derived by benchmarking urban LST values against rural LCZs. Unsupervised K-means clustering was then used to generate compound spatial typologies, revealing four distinct urban risk profiles. Results show that LCZs 4, 5, and 8 host the highest risk zones, where intense thermal stress overlaps with sensitive populations. The framework provides a replicable, high-resolution approach for mapping heat vulnerability and informs targeted adaptation strategies in Mediterranean and climate-vulnerable cities worldwide.

✉ Dyna Chourouk Zitouni
dynachourouk.zitouni@univ-biskra.dz

[1] Laboratory of Design and Modeling of Architectural and Urban Forms and Ambiances (LACOMOFA), University of Biskra, Biskra 07000, Algeria

[2] Department of Architecture, Mohamed Khider University, Biskra 07000, Algeria

[3] Sustainable Building Design Lab, Department UEE Applied Sciences, University of Liège, Liège, Belgium

[4] Department of Architecture, Dar Al-Hekma University, Jeddah, Saudi Arabia

[5] Civil Engineering and Hydraulics Laboratory, Sustainable Development and Environment (LARGHYDE), University of Biskra, Biskra, Algeria

[6] The IDEC Institute and Network for Education and Research on Peace and Sustainability (NERPS), Hiroshima University, Hiroshima, Japan

Published online: 17 October 2025

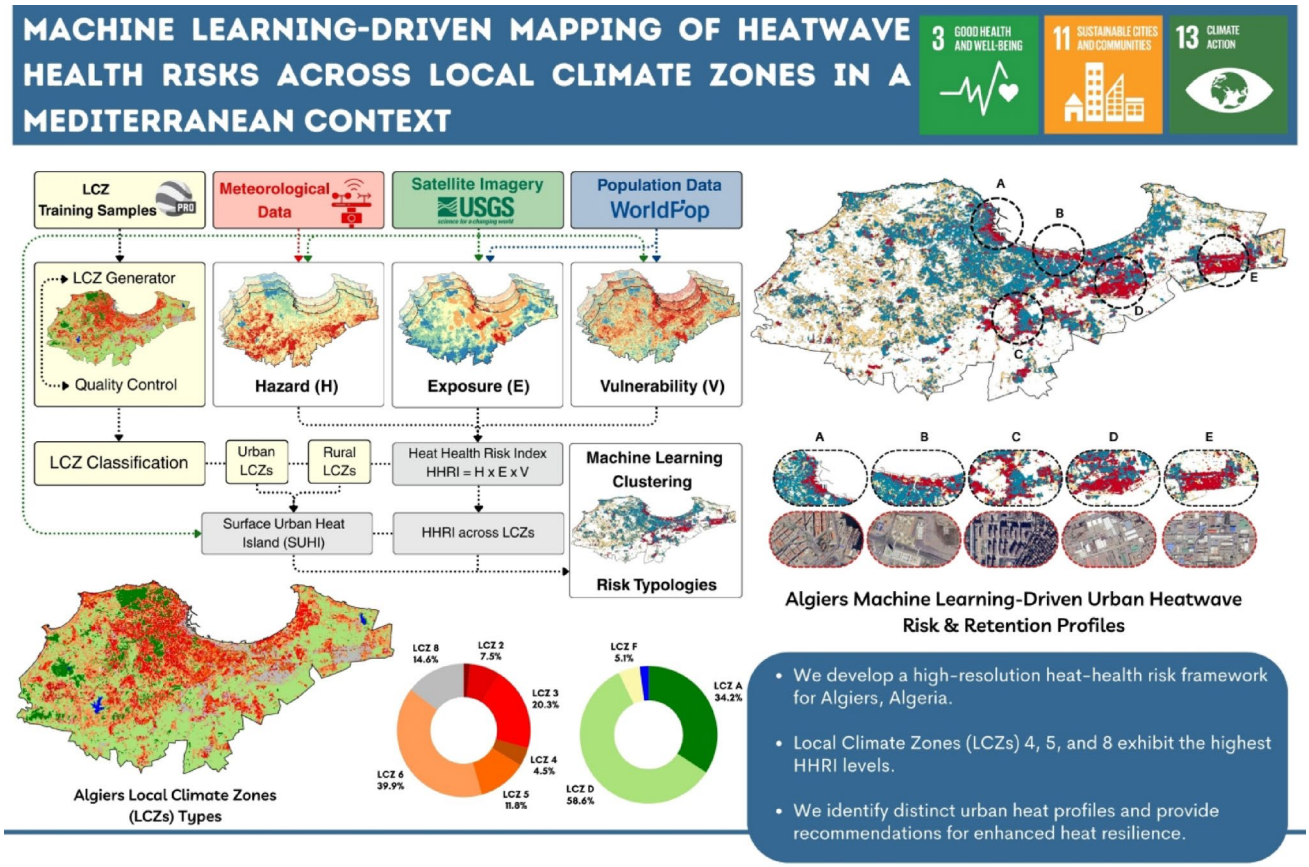

Highlights

- We develop a high-resolution heat-health risk framework for Algiers, Algeria.
- It integrates Heat Health Risk Index (HHRI) and Surface Urban Heat Island (SUHI) metrics.
- Local Climate Zones (LCZs) 4, 5, and 8 exhibit the highest HHR levels.
- LCZs 4, 6, and 8 register the most intense surface heat accumulation.
- We identify distinct urban heat profiles and provide recommendations for enhanced heat resilience.

Keywords Heat health risk index · Surface urban heat island · Climate resilience · Heat vulnerability · LCZ-based risk · Extreme heat.

Abbreviations

Csa	Mediterranean Climate (Köppen classification)
GEE	Google Earth Engine
HHRI	Heat Health Risk Index
HHR	Heat-Health Risk
IPCC	Intergovernmental Panel on Climate Change
LCZ	Local Climate Zone
LST	Land Surface Temperature
ML	Machine learning
MNDWI	Modified Normalized Difference Water Index
MTL	Metadata (Landsat)
NDBI	Normalized Difference Built-up Index
NDVI	Normalized Difference Vegetation Index
OBIA	Object-Based Image Analysis
PCA	Principal Component Analysis
SUHI	Surface Urban Heat Island
UHI	Urban Heat Island
WUDAPT	World Urban Database and Access Portal Tools

1 Introduction

1.1 Study Background

Urban areas are increasingly vulnerable to extreme heat events due to various factors, including climate change and

rapid land surface changes resulting from differences in land cover, building density, and surface materials. To capture this variability, the Local Climate Zone (LCZ) classification system was introduced by Stewart and Oke (2012). Providing a globally consistent framework for categorizing both urban and natural landscapes based on physical and design properties. The system consists of 17 distinct classes, with LCZ 1–10 representing built types and LCZ A-G representing natural or non-built environments (Demuzere et al. 2020). This typology allows cross-city comparisons and supports spatial analysis of heat exposure, land surface temperature (LST), and climate-responsive planning (Huang et al. 2023). Several recent studies have adopted the LCZ framework using the World Urban Database and Access Portal Tools (WUDAPT) methodology, which leverages satellite imagery and open-source tools to generate standardized LCZ maps across diverse global cities (Bechtel et al. 2015; Ching et al. 2018; Ferreira and Duarte 2019).

One of the most widely used applications of the LCZ framework is in analyzing the Surface Urban Heat Island (SUHI), which refers to the temperature difference between urban areas and their surrounding rural zones, as measured by satellite-derived land surface temperatures (LST). SUHI reflects how different urban forms retain and emit heat, offering key insights into the thermal performance of cities (Deng et al. 2024). When combined with LCZs, SUHI provides a refined understanding of how urban morphology influences the spatial distribution of surface heat (Zhao et al. 2021; Rahmani and Sharifi 2024). As highlighted by Zhou et al. (2020), this integration provides a more nuanced understanding of how built environments contribute to surface temperature variation. Verdonck et al. (2018) also underline that accurately mapped LCZs serve as reliable proxies for urban thermal behavior, reinforcing the value of the SUHI-LCZ in urban climate studies.

In Algeria, recent studies have also demonstrated the value of GIS-based multi-criteria analysis in addressing environmental risks, further supporting the relevance of spatial frameworks for climate change assessments (Benmakhlouf et al. 2024; Hadji et al. 2025; Ben Ratmia et al. 2025). Risk monitoring research commonly adopts the hazard–exposure–vulnerability framework, first introduced by Crichton (1999) and later formalized by the Intergovernmental Panel on Climate Change (IPCC) in its Sixth Assessment Report (2021) (IPCC 2021). Within this framework, hazard refers to the occurrence of extreme heat, which exposes the population or infrastructure to risk, and vulnerability refers to the susceptibility of being adversely affected. Together, these components provide a spatial lens for assessing Heat Health Risk (HHR) and identifying priority areas for intervention. Their integration enables quantification of heat stress distribution across urban areas, offering more precise guidance for targeted adaptation measures.

1.2 Literature Review

1.2.1 Machine Learning in Urban Heat-Health

Machine learning (ML) techniques are increasingly being adopted in urban climate research to enhance the accuracy, resolution, and scalability of heat vulnerability and health risk assessments. These methods offer notable advantages in capturing complex, non-linear relationships among environmental, demographic, and spatial variables, enabling predictive modeling, spatial pattern detection, and decision-support capabilities across diverse urban contexts (Zhang et al. 2024). However, despite this growing body of work, the integration of ML into urban heat-health research remains insufficient. Berrang-Ford et al. (2021) conducted a large-scale, ML-enabled review of over 15,000 climate-health articles, finding that most global research remains concentrated on impact assessments, with a limited focus on decision-oriented frameworks. Their findings also reveal significant geographic imbalances, with limited representation from low-income and climate-vulnerable regions, including North Africa and the Mediterranean. The authors stress that, while ML is a powerful tool for organizing and synthesizing vast climate-health knowledge, its full potential remains underutilized, particularly for addressing emerging risks from urban heat exposure. To move beyond static assessments, future research should actively leverage ML frameworks to build spatially explicit and forward-looking urban climate resilience systems.

In parallel, Li et al. (2023) highlighted the transformative potential of integrating ML with remote sensing (RS) for urban sustainability. Their systematic review highlighted that while ML-RS integration has enabled highly accurate image processing and spatial analytics, most studies focus on physical attributes and rely on conventional satellite or aerial imagery. Other dimensions remain underrepresented, and unsupervised learning approaches are still underutilized.

Initial progress has been made in this direction, as several studies have begun to demonstrate the capacity of ML to model heat-related health risks at varying spatial and temporal scales. Notably, Boudreault et al. (2024) developed a multi-region ML framework to predict multiple heat-related health outcomes in Quebec, Canada. Their approach enabled generalized and scalable prediction across regions, utilizing meteorological and socio-temporal features. Similarly, J. Wang et al. (2024a, b) applied a multi-scale ML model to estimate and project heat-related mortality in Germany, linking high-resolution climate and health datasets with socioeconomic pathways to inform both real-time warnings

and long-term public health strategies. From a health-oriented urban climate perspective, Y. Zhou and Wan (2025) combined LST, infectious disease trends, and spatial data in Beijing to identify cold and heat risk zones using ML models that evaluated the influence of urban morphology, land use, and human activity.

Urban-scale assessment studies have also benefited from machine learning's ability to manage multi-source spatial data. One example is the U-HEAT framework introduced by Li et al. (2024), which combines ML) and remote sensing for policy-driven heat vulnerability analysis, and supports continuous model improvement through active learning. In another case, Random Forest algorithms were applied to assess heat vulnerability across Australian capital cities, revealing personal health and demographic factors as key predictors **(**Li et al. 2025). Similarly, a study in Wuhan, China, utilized three ML models to distinguish between day and night heat hotspot patterns, demonstrating that different urban features drive each, and offering insights for improved heat planning Liu et al. (2025). These data-driven approaches underscore a growing methodological shift from static, indicator-based frameworks to ML-enabled systems that support ongoing refinement, broader generalization, and operational decision-making.

1.2.2 LCZ-Based Heat Health Risk Framework

An emerging line of research has begun coupling the Heat Health Risk (HHR) framework with Local Climate Zone (LCZ) classifications, enabling a morphology-based understanding of heat exposure and vulnerability in urban environments.

A foundational contribution was led by Ma et al. (2023), who conducted a multi-year study (2015–2020) in Changzhou, China, during the summer months. The authors integrated LST, high-temperature frequency, and nighttime temperature patterns with demographic and environmental variables to evaluate urban heat risk. Xiang et al. (2024) extended this approach across three major Chinese cities (Wuhan, Nanjing, and Shanghai), focusing on SUHI intensity and population exposure during the summer periods of 2010, 2015, and 2020. Also, Yang et al. (2024) adopted a seasonal perspective in Shanghai, examining thermal exposure from spring 2020 to winter 2022 using the Modified Temperature-Humidity Index, along with surface cover data and built environment characteristics.

Similarly, Su et al. (2024) evaluated summer periods in 2020 and 2022 in Shenzhen, China, using MTHI and demographic indicators to assess child heat vulnerability. Meanwhile, Zou et al. (2024) focused on Guangzhou from July to August 2015–2020, incorporating LST, anthropogenic heat flux, and elderly population density to characterize urban thermal health risks. More globally comparative research by Yu et al. (2024) analyzed several megacities (Beijing, Cairo, Jakarta, Mumbai, Rio de Janeiro, and Tehran) during short but intense heatwave windows in 2020. The article relied on spatial population datasets, environmental indicators, and accessibility metrics to hospitals. Moreover, development (Erlwein and Pauleit 2021). expanded the analysis to major cities throughout China, using long-term summer data (2000–2020) and applying multiple climatic indicators, including high-temperature frequency, wind speed, and humidity, along with vulnerability data. Moving beyond China, Baqa et al. (2025) explored heat risk in Karachi, Pakistan, during the 2022 heatwave, combining LST with built environment indicators such as slum coverage and utility access. Most recently, Guo et al. (2025) conducted research in the summer of 2023 in Qingdao, China, integrating SUHI data with population exposure to map urban thermal risk using clustering methods. Table 1 provides a comparative overview of the existing studies that have integrated HHR components within the LCZ framework, highlighting their spatial focus, analysis periods, and data inputs.

Despite the success of recent efforts by Xiang et al. (2024) and Guo et al. (2025) in integrating the SUHI index as a hazard component within the HHRI, important limitations remain. Treating SUHI as just one part of the hazard component assumes it contributes to risk in a uniform and fixed manner. This can overlook how surface heat interacts with other risk factors, such as population vulnerability or exposure patterns. Instead, analyzing SUHI and HHRI as two separate layers and then combining them through clustering methods allows for a more comprehensive understanding of where extreme surface heat overlaps with high heat risk. This approach helps identify areas facing the most critical combination of thermal and social vulnerability, providing insights that are often missed when SUHI is embedded within a single index.

1.3 Research Gab and Study Objectives

While early applications of the hazard–exposure–vulnerability framework in HHR research were relatively limited (Ye and Yang 2025), their number is expanding progressively, with a strong research focus emerging across various Asian contexts. Despite this progress, major gaps remain in the methodological integration of key indicators. Most notably, the combined use of HHRI and SUHI through machine learning–based clustering remains underutilized in heat risk research.

In this context, the integration of HHRI assessments within the LCZ framework remains insufficiently explored. Although LCZ classification enables fine-grained differentiation of heat exposure based on urban morphology, its

Table 1 Overview of studies on Heat-Health risk assessment across LCZs

Authors, Year	Study Area	Climate Zone (Köppen)	Study Period	HHRI Components			LCZ Method	LCZ at Higher Risk
				Hazard	Exposure	Vulnerability		
Ma et al. 2023	Changzhou, China	Cfa	Summer (2015–2020)	LST, High Temp. Frequency	Population Density, High Temp. Frequency	Elderly population (+65), NDVI, MNDWI, Nighttime lights	OBIA with Multi-Source Data	LCZ 1 LCZ 3
Xiang et al. 2024	Wuhan, Nanjing, Shanghai (China)	Cfa	July–August (2010, 2015, and 2020)	SUHI	Population, Nighttime Light	Elderly population (+65)	WUDAPT method via LCZ Generator	LCZ 1 LCZ 2
Yu et al. 2024	Beijing, Cairo, Jakarta, Mumbai, Rio de Janeiro, Tehran	Cwa, BWh, Af, Aw	City-specific heatwave windows: Feb–Dec 2020 (3-day periods)	LST	Population Density	Nighttime lights, Road density, EVI, Distance to hospitals	LCZ maps from Demuzere et al. (2022)	LCZ 1 LCZ 2
Zou et al. 2024	Guangzhou, China	Cfa	July–August (2015–2020)	LST, Anthropogenic Heat Flux	Population Density, NDVI, Enhanced Water Index (EWI)	Elderly population (+65), Nighttime lights	GIS-based LCZ classification using fuzzy logic + majority voting	LCZ 1 LCZ 4
Su et al. 2024	Shenzhen, China	Cfa	Summer (2020 and 2022)	Modified Thermal–Humidity Index (MTHI)	Population Density, Impervious Surface Area	Elderly population (+65), Young population (−15)	LCZ map from WUDAPT, combined with 1 m Land Cover	LCZ 2 LCZ 8
Yang et al. 2024	Shanghai, China	Cfa	Spring, Summer, Autumn, Winter (2020–2022)	LST, MNDWI	Population Density + Impervious Surface Area	Elderly population (+65), Young population (−15), % of water and vegetation	Decision tree-based GIS LCZ Classification	(Summer) LCZ 2 LCZ 8
Baqa et al. 2025	Karachi, Pakistan	BWh	May 2022 (heatwave period)	LST	Population Density	Elderly population (+65), Young population (−10), Illiterate population, Housing density, Slum dwellers, Houses with access to potable water-Bathrooms-Electricity, Children with large families, Poverty rate, NDVI	WUDAPT method via LCZ Generator	LCZ 2 LCZ 3
Zhang et al. 2025	Urumqi, Shenyang, Tianjin, Wuhan, Nanjing, Chongqing (China)	Dfa, Dwa, Cfa, Cwa	Summer (2000, 2010, and 2020)	LST, High Temp. Frequency, Humidity, Wind speed	Population Density, High Temp. Frequency	Elderly population (+80), Young population (−4), Nighttime lights, NDVI, MNDWI, Air quality	National LCZ dataset	LCZ 1 LCZ 4
Guo et al. 2025	Qingdao, China	Dwa	June–August (2021–2023)	SUHI	Population Density, POI, Roads	Elderly population (+65), Young population (−15), Housing price, GDP, Medical facilities, Cooling shelter, Distance from coastline and green space	K-means++ + Stacking (SVM, RF)	LCZ 1 LCZ 2

potential remains underutilized when integrated with HHR modeling frameworks. In parallel, there is a notable geographic imbalance in literature.

A very recent study by Matallah et al. (2025), which analyzed 30 years of heating and cooling degree days, underscores the climatic complexity of North Africa and the urgent need for localized thermal adaptation strategies. However, most existing studies remain concentrated in East and Southeast Asia, with limited application in North African and Mediterranean contexts. This gap is particularly concerning for highly exposed countries like Algeria, where only one recent study by Zitouni et al. (2025) has applied the HHRI framework at a municipal scale. While it provided valuable insights, it lacked the high spatial resolution required to inform localized urban heat adaptation. How can the integration of HHRI and SUHI within the LCZ framework, supported by unsupervised machine learning, enhance spatial typologies of heat-health risk in Mediterranean cities like Algiers?

Bridging these gaps is crucial for developing targeted, evidence-based heat risk strategies in vulnerable and data-scarce urban areas. Accordingly, this research aims to fill these gaps through the following objectives:

(1) Analyze SUHI intensity across LCZs using multi-year satellite-derived LST data (2015–2023).

(2) Map heat-health risks across LCZs in Algiers using the IPCC-based HHRI framework for the same period.

(3) Apply machine learning clustering to combine HHRI and SUHI, identifying spatial typologies of compounded heat risk.

This article aims to provide the first comprehensive assessment of heat-related health risks and surface thermal intensity in Algiers within the LCZ framework. By combining remote sensing, demographic data, and unsupervised clustering, it addresses a critical research gap in the region. The resulting compound typology of SUHI and HHRI supports spatially targeted adaptation strategies. The proposed methodology is applicable to other urban contexts and offers valuable insights for climate-resilient planning in Mediterranean and data-scarce cities.

2 Methodology

This methodology integrates remote sensing, geospatial analysis, and machine learning to assess heat health risks across Local Climate Zones (LCZs). As illustrated in Fig. 1, the workflow involves data acquisition, LCZ classification, HHRI and SUHI computation, and multivariate clustering to identify spatial patterns of heat vulnerability and

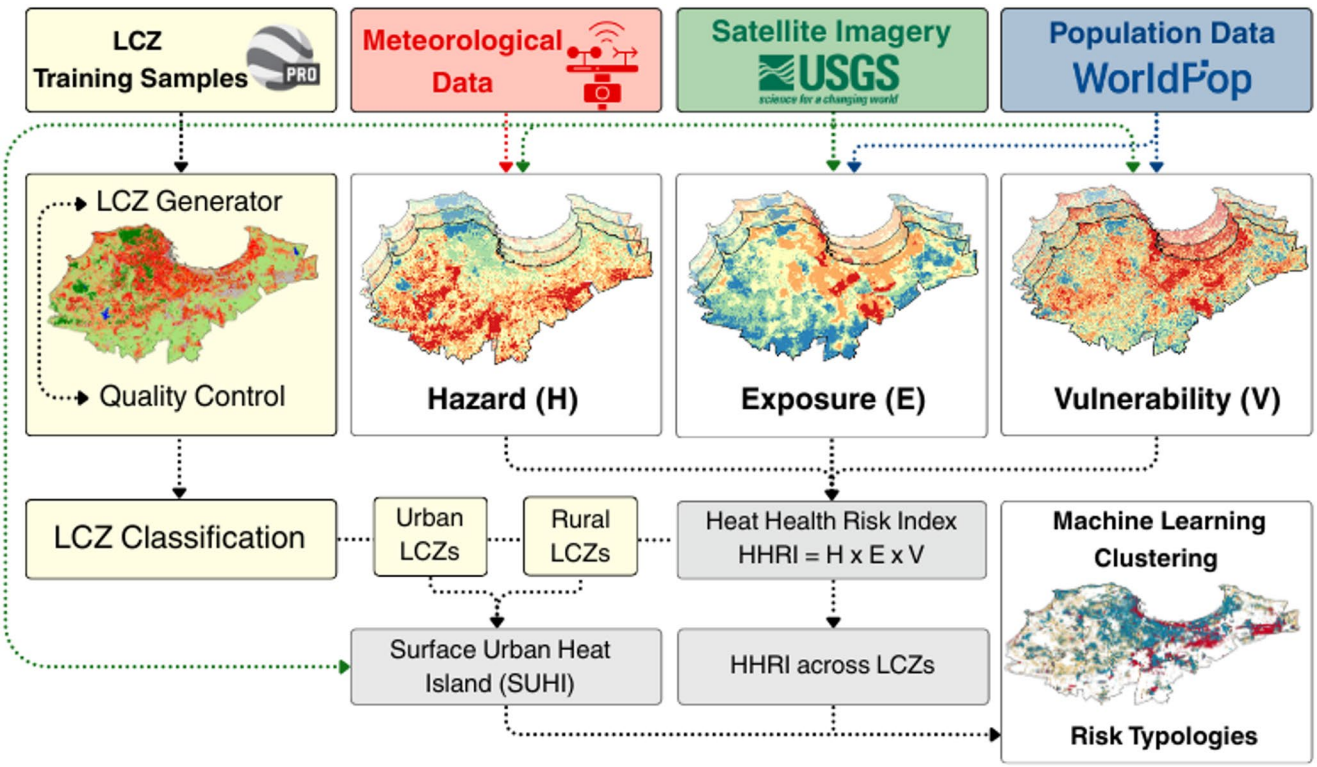

Fig. 1 Methodology conceptual framework

intensity. The proposed methodology is applicable to other urban contexts and offers valuable spatial insights based on satellite-derived and vulnerability data.

2.1 Data Acquisition

This research focuses on Algiers, the capital of Algeria (36°46′34″ N, 3°03′36″ E), which spans 80 km of coastline with varied topography. The city has a Mediterranean (Csa) climat, characterized by long, hot, and dry summers, during which temperatures often exceed 40 °C. As Algeria's most densely populated province, with 3.3 million residents across 57 municipalities (as of 2020), Algiers presents a relevant case for examining urban heat stress and associated health risks. The administrative boundaries and topographical context of the research area are illustrated in Fig. 2.

The data sources include manually labeled LCZ training samples extracted from Google Earth Pro V 7.3.6, global population datasets (WorldPop 2023), satellite imagery from the United States Geological Survey (USGS), and meteorological data from Algiers's national weather stations spanning the period from 2015 to 2023 (Zitouni et al. 2024) (Dataset). Table 2 summarizes the dataset, acquisition dates, resolution, and sources.

LCZs were mapped using manually digitized training samples in Google Earth Pro following the WUDAPT

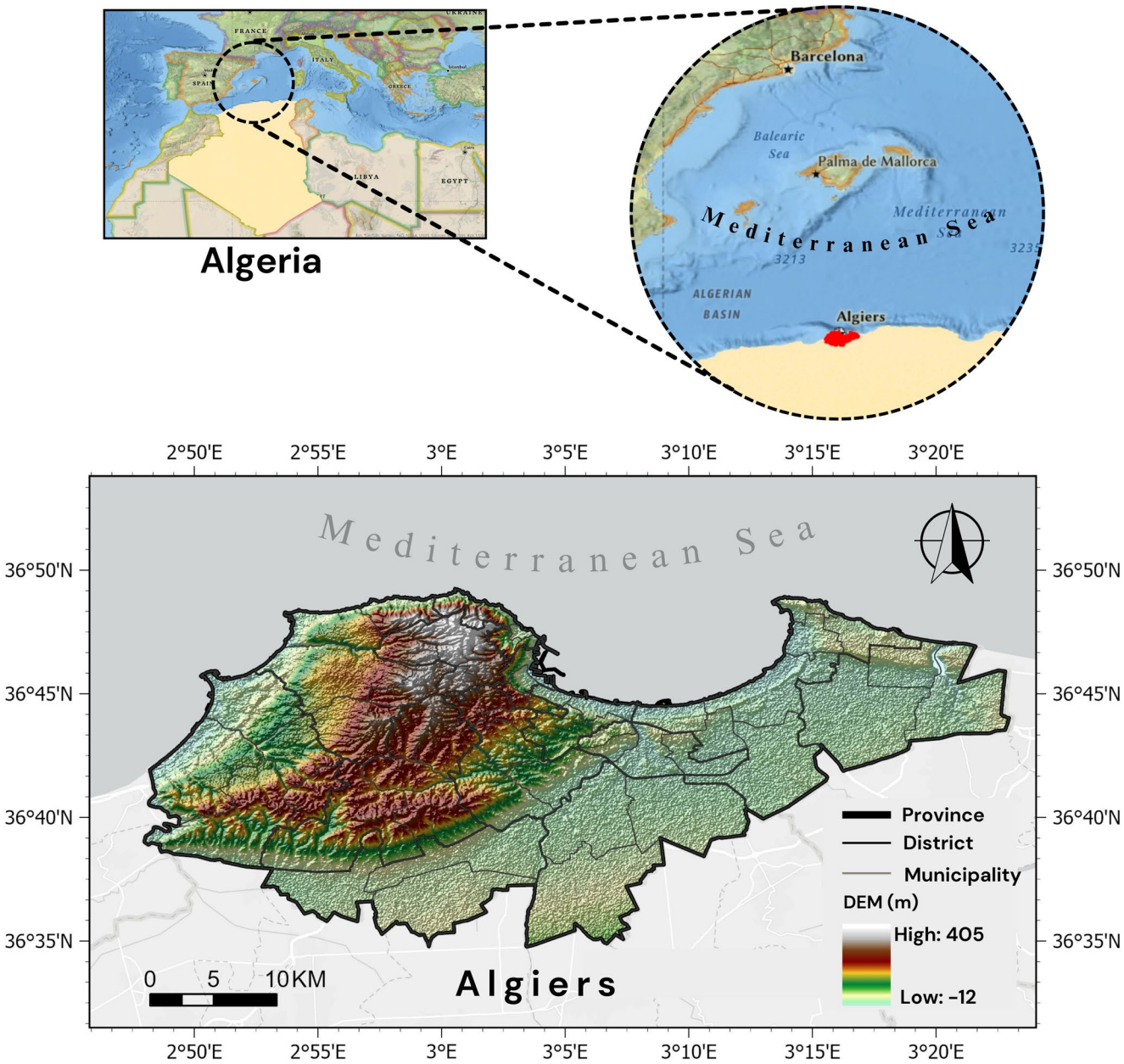

Fig. 2 Research Area

Table 2 Datasets

Type	Description	Period	Resolution	Source
LCZ Training Samples	Manually digitized polygons for LCZ classification	2023	~100 m (final LCZ output)	Google Earth Pro v7.3.6
Population Data	Gridded population, including < 15 and > 65 years age groups	2020	100 m	WorldPop (https://www.worldpop.org/)
Satellite Imagery	Landsat 8 & 9 for LST, NDVI, NDBI, MNDWI indices	2015–2023	30 m	USGS Earth Explorer (https://earthexplorer.usgs.gov/)
Meteorological Data	Daily Max air temp. to extract heatwaves and hot days	2015–2023	Station-level	National Weather Stations—Algiers

method (Bechtel et al. 2015). Training polygons were selected to ensure representative LCZ coverage and classification accuracy. Population data from WorldPop (2023) provided 100 m resolution estimates for total and age-specific groups, spatially aligned with LCZs. Landsat 8 and 9 imagery (2015–2023) from USGS was used to compute LST, NDBI, NDVI, and MNDWI using cloud-free images during heatwave days. Meteorological data from national stations provided daily maximum temperatures, from which heatwaves (≥3 consecutive days with temperatures exceeding 35 °C) and hot days (>35 °C) were derived to complement satellite-based thermal assessments.

2.2 LCZ Classification

In this research, LCZ mapping was performed using the LCZ Generator (Demuzere et al. 2021), an open-access semi-automated tool aligned with the WUDAPT Level 0 protocol. The process combines remote sensing data with supervised machine learning. Training areas were manually selected in Google Earth Pro to represent each LCZ class, following Demuzere et al. (2021) guidelines to ensure spatial coverage, internal consistency, and representativeness. Local knowledge and geospatial data supported the verification process, informing the subsequent classification carried out using the Random Forest algorithm in Google Earth Engine. This model leveraged spectral, textural, and structural variables. The resulting LCZ map was evaluated using standard accuracy metrics, including overall accuracy, user's and producer's accuracy, and the kappa coefficient.

2.3 Heat Health Risk Index (HHRI) Assessment

To evaluate heat-related risk spatially, the HHRI framework incorporates indicators of thermal intensity, population exposure, and environmental sensitivity, allowing for risk mapping across different LCZs.

First, the hazard component captures extreme heat patterns using satellite and meteorological data. LST reflects surface heat intensity, while heatwave and hot day frequencies (2015–2023) were derived from national weather station records. Building on this, the exposure dimension represents the extent to which the population and infrastructure are subjected to heat. It combines population density and NDBI, indicating the prevalence of impervious surfaces. Finally, the vulnerability component accounts for both demographic and environmental susceptibility. Demographic vulnerability includes the percentage of residents under 15 and over 65 years old. Environmental vulnerability is assessed using NDVI and MNDWI, both of which are inversely scaled to account for their cooling effects. A summary of these indicators, along with their calculation methods, is provided in Table 3.

Accordingly, the HHRI is calculated by multiplying the three components following Eq. (1):

$$HHRI = H \times E \times V \tag{1}$$

Table 3 HHRI components

Compenents	Indicators	Description	Formula
Hazard	LST	The temperature of the Earth's surface is measured using satellite images of thermal bands	$LST = \frac{BT}{1+(w \times \rho\, BT) \times ln(\epsilon)}$
	Hot days	Days with maximum air temperatures greater than 35 °C	Count of days with Tair Max > 35 °C
	Heatwave frequency	Number of events where the max daily average temperature exceeds 35 °C for more than 3 days	Count of days with Tair max > 35 °C for more than 3 consecutive days
Exposure	Population density	Population per 100 m	Extracted from WorldPop 2020 raster
	NDBI	An index used to measure built-up areas and urbanization	$\frac{(SWIR - NIR)}{(SWIR + NIR)}$
Vulnerability	NDVI	An index used to measure the density of vegetation	$\frac{(NIR - Red)}{(NIR + Red)}$
	MNDWI	An index used to identify water bodies	$\frac{(NIR - SWIR)}{(NIR + SWIR)}$
	Elderly population	Population over 65 and older per 100 m	Extracted from WorldPop 2020 raster
	Young population	Population aged 15 and less per 100 m	Extracted from WorldPop 2020 raster

All components were normalized using the min-max normalization formula to maintain consistency and comparability following Eq. (2):

$$Xnorm = \frac{\boldsymbol{X} - \boldsymbol{X}min}{\boldsymbol{X}max - \boldsymbol{X}min} \quad (2)$$

Where $Xnorm$ represents the normalized value, $\boldsymbol{X}$ is the original value, and $\boldsymbol{X}min$ and $\boldsymbol{X}max$ are the minimum and maximum values in the dataset, respectively.

To ensure a reliable and unbiased HHRI construction, Principal Component Analysis (PCA) was used to assign weights to each variable, minimizing multicollinearity and enhancing indicator reliability. Weighted components were aggregated across LCZs in ArcGIS Pro, with HHRI values classified into five risk levels.

2.4 Surface Urban Heat Island (SUHI) Calculation across LCZs

The SUHI effect refers to the temperature difference between urbanized and surrounding non-urbanized areas, typically observed through remotely sensed LST data (Zhou et al. 2018). In this research, SUHI intensity was calculated to quantify differences in surface thermal conditions across the LCZs identified in Algiers. LST data were derived from Landsat 8 and 9 thermal infrared bands for the summer period spanning 2020 to 2023. Raw imagery was processed via radiative transfer to derive LST with NDVI-based emissivity correction.

To quantify SUHI intensity, a zonal statistics approach was used. Mean LST values were calculated for each LCZ in ArcGIS Pro. Natural LCZs (A, D, F, and G) served as rural reference zones, providing baseline temperatures against which urban LCZs (LCZ 1 to LCZ 8) were compared using Eq. (3):

$$SUHI = LST_{LCZi} - LST_{Rural} \quad (3)$$

Where $LST_{LCZi}\, is$ the mean LST of the urban LCZ class i and LST_{Rural} represents the mean LST of the combined rural LCZ classes.

2.5 HHRI and SUHI Clustering Analysis

SUHI and HHRI were integrated using unsupervised machine learning within the LCZ framework. K-means clustering was selected for its efficiency and suitability for multivariate spatial analysis, a method widely used in urban and environmental studies to uncover latent spatial patterns. The clustering process began by calculating average SUHI and HHRI values for each LCZ class using zonal statistics in ArcGIS Pro. These indicators were chosen for their complementarity: SUHI reflects thermal intensity linked to urban form, while HHRI captures population vulnerability and adaptive capacity.

Each LCZ class was represented as a data point in a two-dimensional feature space following Eq. (4):

$$X = \{(x_i,\, y_i)\}_{i=1}^{n} \quad (4)$$

Where x_i is the normalized SUHI value and y_i the normalized HHRI value for LCZ i, and n is the total number of LCZ classes considered.

The K-means algorithm was applied to classify the data into clusters by minimizing intra-cluster variance. The optimal number of clusters was determined using the Elbow Method based on the within-cluster sum of squares (WCSS). Four distinct composite risk typologies emerged:

1. High HHRI – High SUHI: Areas facing both extreme thermal exposure and high vulnerability require urgent intervention.
2. High HHRI – Low SUHI: Zones with moderate heat levels but high social sensitivity, highlighting vulnerability-driven risk.
3. Low HHRI – High SUHI: Hot areas with low vulnerability, typically non-residential or better-resourced environments.
4. Low HHRI – Low SUHI: Thermally and socially resilient zones with favorable microclimatic and demographic conditions.

These clusters were mapped using ArcGIS Pro, providing spatially explicit insights to guide targeted urban heat adaptation strategies.

3 Results

3.1 LCZ Classification

The final LCZ map (Fig. 3) reveals the spatial distribution of urban and natural land cover types, providing a foundation for assessing their relationship with heat-related risks.

The LCZ classification yielded an overall accuracy of 89.12% and a Kappa coefficient of 0.83. The spatial analysis indicates that urban built-up LCZs, particularly compact and open configurations, are predominantly concentrated in the coastal and central districts of Algiers. These zones correspond to areas of dense human activity and infrastructure, often with high levels of impervious surfaces and limited vegetation. In contrast, natural land cover zones, including forested, vegetated, and undeveloped areas, are more

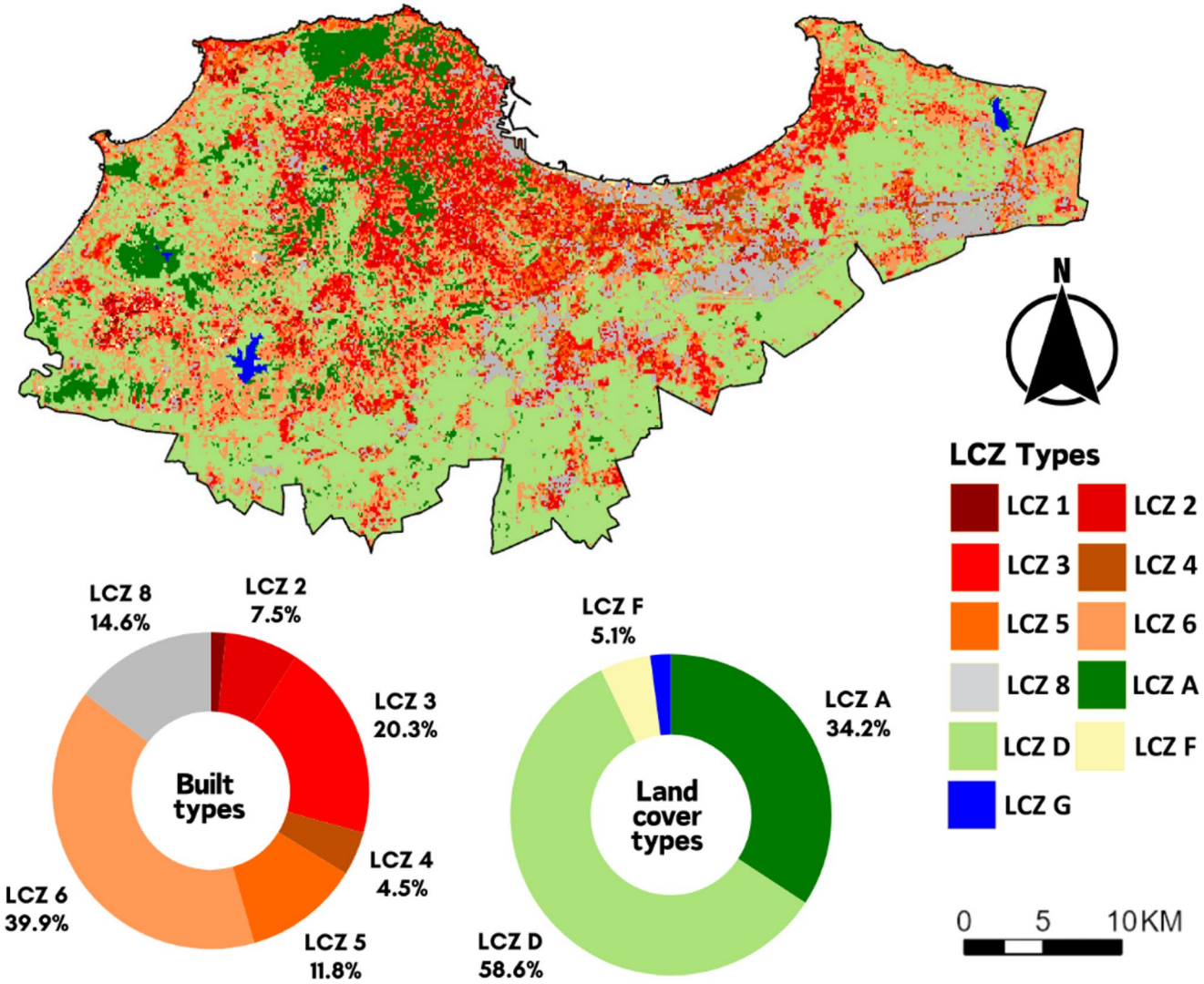

Fig. 3 Algiers LCZ spatial distribution and proportions (2023)

prevalent in the southern and peripheral parts of the city, where topographical constraints and lower development pressure have preserved green space.

Among the built-up LCZs, LCZ 6 (Open Low-rise) emerges as the most widespread urban typology, covering approximately 39.9% of the total classified area. This typology typically includes low-rise residential buildings interspersed with open space, resulting in varying levels of population exposure. LCZ 3 (Compact Low-rise) follows with a coverage of 20.3%, representing older neighborhoods with tighter building arrangements and reduced ventilation capacity. Other built categories, including LCZ 2 (Compact Mid-rise), LCZ 5 (Open Mid-rise), and LCZ 4 (Open High-rise), occupy smaller proportions, reflecting less vertical expansion and a lower overall footprint in the urban structure. Notably, LCZ 1 (Compact High-rise) is the least represented among the built classes, pointing to limited occurrences of dense high-rise clusters in the city's urban landscape. This uneven spatial distribution of LCZ types mirrors the historical and socioeconomic development trajectories of Algiers, where informal growth and zoning constraints have shaped a predominantly low- to mid-rise urban fabric.

Regarding natural land cover, LCZ D (Low Plants) occupies the largest proportion (58.6%), indicating the presence of significant green spaces, followed by LCZ A (Dense Trees), covering 34.2% of the research area. Water bodies, represented by LCZ G (Water), cover a minimal fraction, highlighting the limited presence of cooling blue surfaces.

The classification results suggest a strong urban-rural gradient, with high-density urban areas concentrated in the north and more vegetated landscapes towards the south. This spatial variability in urban morphology and land cover is expected to influence HHR and urban heat patterns.

3.2 HHR Assessment

3.2.1 Hazard Index

The hazard component (Fig. 4a) quantifies the intensity and frequency of extreme heat events. The highest hazard levels are predominantly observed in dense urban areas, particularly in LCZ 8 (Large Low-rise) and LCZ 6 (Open Low-rise), where elevated LST values, frequent hot days, and recurring heatwaves contribute to increased thermal stress. These built-up forms, characterized by limited vegetation and expansive impervious surfaces, amplify surface heat retention. Notably, LCZ 8 recorded the highest proportion of "very high" hazard values at 29%, followed by LCZ D (Low Plants) at 23%, LCZ 6 at 17%, LCZ F (Bare soil or sand) at 9%, and LCZ 2 (Compact Mid-rise) at 6%. In contrast, LCZ A (Dense Trees) and LCZ G (Water Bodies) exhibit significantly lower hazard values, highlighting the cooling benefits of vegetated and water-covered zones. The bar chart (Fig. 4b) confirms that LCZs 8, 6, and D are the most hazard-prone, while A and G function as important thermal moderators in the urban landscape.

3.2.2 Exposure Index

The exposure component (Fig. 4c) represents the extent to which populations and built environments are subjected to extreme heat conditions. The highest exposure values are observed in high-density residential and commercial zones, particularly in LCZ 2 (Compact Mid-rise), LCZ 4 (Open High-rise), and LCZ 5 (Open Mid-rise), where elevated population densities, extensive impervious surfaces, and limited shading contribute to heightened thermal exposure. LCZ 2 and LCZ 4 recorded the highest proportions of "high" exposure, accounting for 44% and 43%, respectively, while also showing notable shares of "very high" exposure at 11% each, alongside LCZ 5. LCZ 8 (Large Low-rise) and LCZ 3 (Compact Low-rise) followed with 10% and 8% in the "very high" class, indicating their growing role in population exposure. The bar chart (Fig. 4d) reflects these distributions across built-up forms. In contrast, LCZ A (Dense Trees), LCZ D (Low Plants), and LCZ G (Water Bodies) display predominantly "low" or "very low" exposure levels, consistent with their sparse human occupation and more natural land cover types.

3.2.3 Vulnerability Index

The vulnerability component (Fig. 4e) accounts for demographic and environmental factors that increase susceptibility to heat stress. Higher vulnerability levels are concentrated in areas with a high proportion of elderly and young populations, as well as areas with limited vegetation cover. Among built-type zones, LCZ 1 (Compact High-rise), LCZ 2 (Compact Mid-rise), and LCZ 8 (Large Low-rise) represent the most vulnerable classes, mainly due to the presence of heat-sensitive populations and reduced green space. As illustrated in the bar chart (Fig. 4f), LCZ F had the highest overall proportion of "very high" vulnerability level at 80%, followed closely by LCZ 1 and LCZ 2 (both at 76%) and LCZ 8 at 73%. Mid-level vulnerabilities were observed in LCZ 3 (64%) and LCZ 5 (55%), while LCZ 4 and LCZ 6 recorded lower levels at 45% and 32%, respectively. In contrast, LCZ A had the lowest vulnerability share at only 6%, followed by LCZ D (dense vegetation) at 9%, and LCZ G (water bodies) at 37%, reflecting the protective influence of natural surfaces and the absence of population exposure.

3.3 HHRI across LCZs

The HHRI map (Fig. 5a) integrates the three components (hazard, exposure, and vulnerability) to provide a comprehensive spatial assessment of HHR across the research area. The results indicate that high-risk areas are primarily concentrated in compact and high-density urban zones, whereas low-risk areas correspond to vegetated and water-rich environments.

The highest HHRI percentages are observed in LCZ 4 (8%), followed by LCZ 5 (7%), LCZ 2 and LCZ 8 (5%), and LCZ 3 (4%), indicating that these areas are the most vulnerable among the built-up classes. These LCZs combine high population densities, impervious surfaces, and limited vegetation, increasing both thermal and health-related risks. In contrast, LCZ B, LCZ F, and LCZ G exhibit the lowest HHRI values, reinforcing the critical role of vegetation and water bodies in reducing heat risk. The bar chart (Fig. 5b**)** further illustrates the distribution of HHRI risk levels within each LCZ, confirming the dominance of high and very high-risk classes in open urban areas. At the same time, vegetated and water-rich zones maintain low-risk profiles. These findings underscore the importance of integrating heat adaptation strategies within high-risk LCZs to enhance urban climate resilience.

This trend aligns with findings from recent studies in Asian cities, where similar LCZ typologies have shown elevated HHRI levels due to a combination of thermal exposure and demographic susceptibility (Su et al. 2024; Yu et al. 2024; Zou et al. 2024). Such alignment reinforces the relevance of LCZ-based assessments in identifying urban HHR across different climatic and geographical settings.

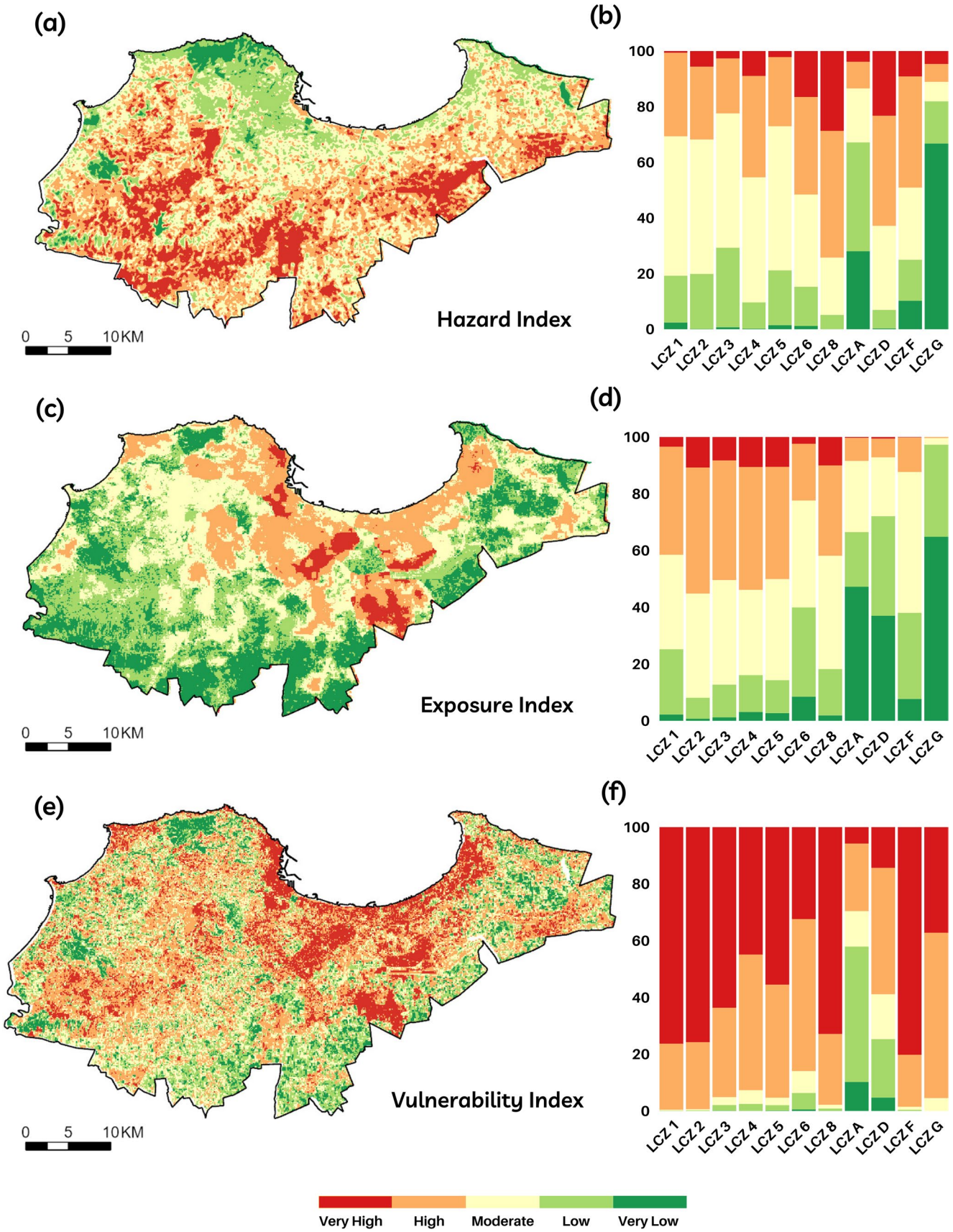

Fig. 4 Spatial distribution of the hazard (**a**), exposure (**c**), and vulnerability (**e**) in Algiers (2015–2023), and their stacked columns by LCZ at different levels (**b**, **d**, **f**)

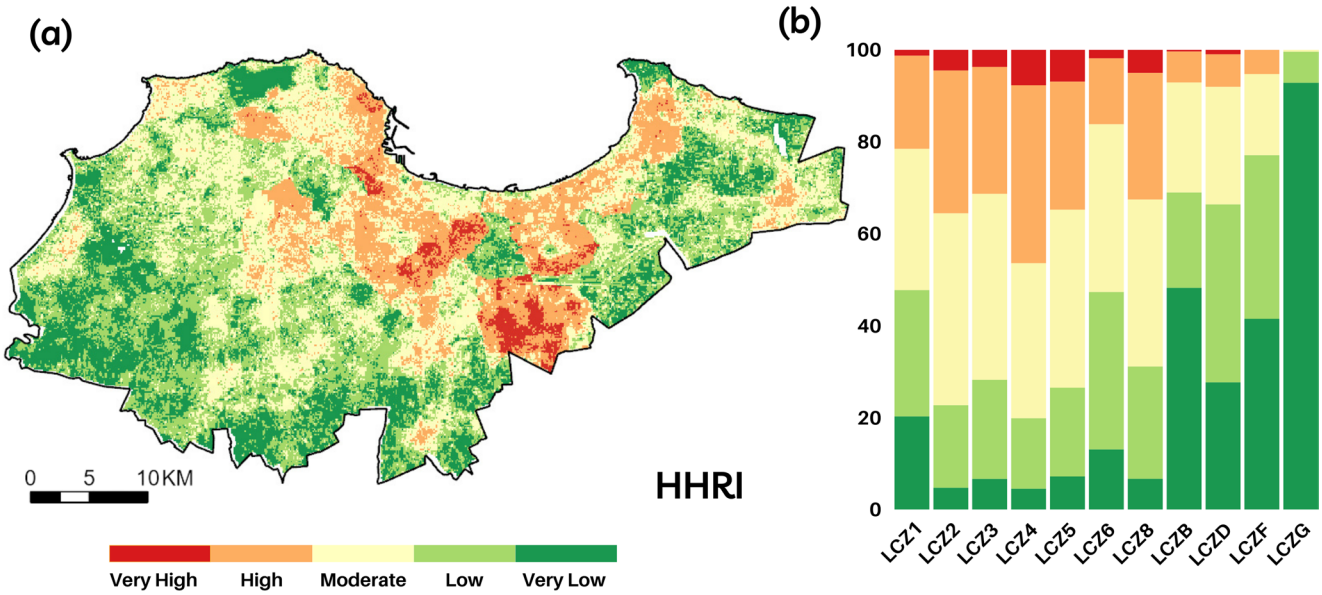

Fig. 5 Spatial distribution of the HHRI in Algiers (**a**) and its stacked columns of LCZ to different levels (**b**)

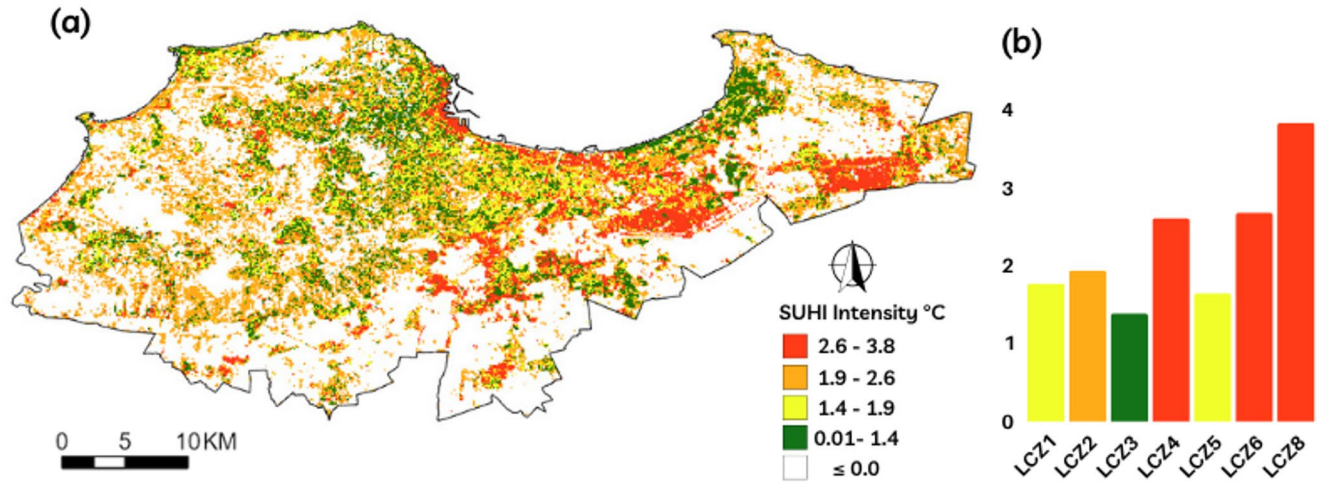

Fig. 6 SUHI Intensity in Algeris (2015–2023) (**a**) and its bar chart across built types LCZs (**b**)

3.4 SUHI Analysis

The SUHI analysis offers insights into spatial heat intensity patterns across various LCZs, based on the mean LST observed between 2015 and 2023. SUHI values were computed by subtracting the average LST of rural LCZs from each urban LCZ. The resulting SUHI raster was classified into five classes using the Natural Breaks (Jenks) method to visualize the intensity of urban heat accumulation (Fig. 6).

The findings reveal a distinct stratification of SUHI intensity across built LCZ types in Algiers. LCZ 8 (Large Low-rise) recorded the highest intensity at 3.83 °C, followed by LCZ 6 (Open Low-rise) with 2.68 °C, and LCZ 4 (Open High-rise) with 2.61 °C. Mid-range values were observed in LCZ 2 (Compact Mid-rise) at 1.94 °C, LCZ 1 (Compact High-rise) at 1.77 °C, and LCZ 5 (Open Mid-rise) at 1.65 °, while LCZ 3 (Compact Low-rise) registered lower values of 1.39 °C.

These results confirm a consistent gradient in surface heat intensity across urban forms. Similar patterns have been reported in Oran, Algeria (Soufiane et al. 2025), where LCZ 8 and other dense types showed elevated SUHI values. The spatial distribution of SUHI intensities (Fig. 6) reveals that the highest values are primarily concentrated in the central and southern sectors of the city. In contrast, lower values are more common in peripheral areas with greater natural land cover.

3.5 Clustering of HHR and Retention Patterns

The integration of HHRI and SUHI through a clustering-based approach enabled the identification of distinct urban thermal risk typologies across Algiers (Fig. 7). This spatial segmentation, derived using a machine learning-driven multivariate clustering algorithm, classified the entire research area into four clusters, each reflecting a unique combination of demographic vulnerability and thermal stress.

Cluster 1 (High SUHI–High HHRI) is mainly concentrated in five key zones across Algiers, as shown in Fig. 7. These include Area A, which encompasses the dense fabric of central Algiers; Area B, covering the public spaces and waterfront areas in front of the Great Mosque of Algiers; Area C, located in the Baraki municipality, known for its residential expansion; Area D, surrounding the Houari Boumediene International Airport and adjacent industrial zones; and Area E, corresponding to the industrial district of Rouiba. These areas collectively represent the most critical hotspots where surface heat retention and population vulnerability converge and therefore, merit urgent attention in adaptation planning.

Cluster 2 (High SUHI–Low HHRI) includes areas with high thermal intensity but lower health risk scores, mostly located in peri-urban and industrial zones, as well as newer urban developments such as Mhelma, Souidania, and Sidi Abdellah. These zones experience substantial heat retention but benefit from relatively lower population vulnerability due to improved infrastructure and newer housing stock. Cluster 3 (Low SUHI–High HHRI) comprises areas with lower surface heat but elevated health-related vulnerability. These are generally situated in demographically sensitive

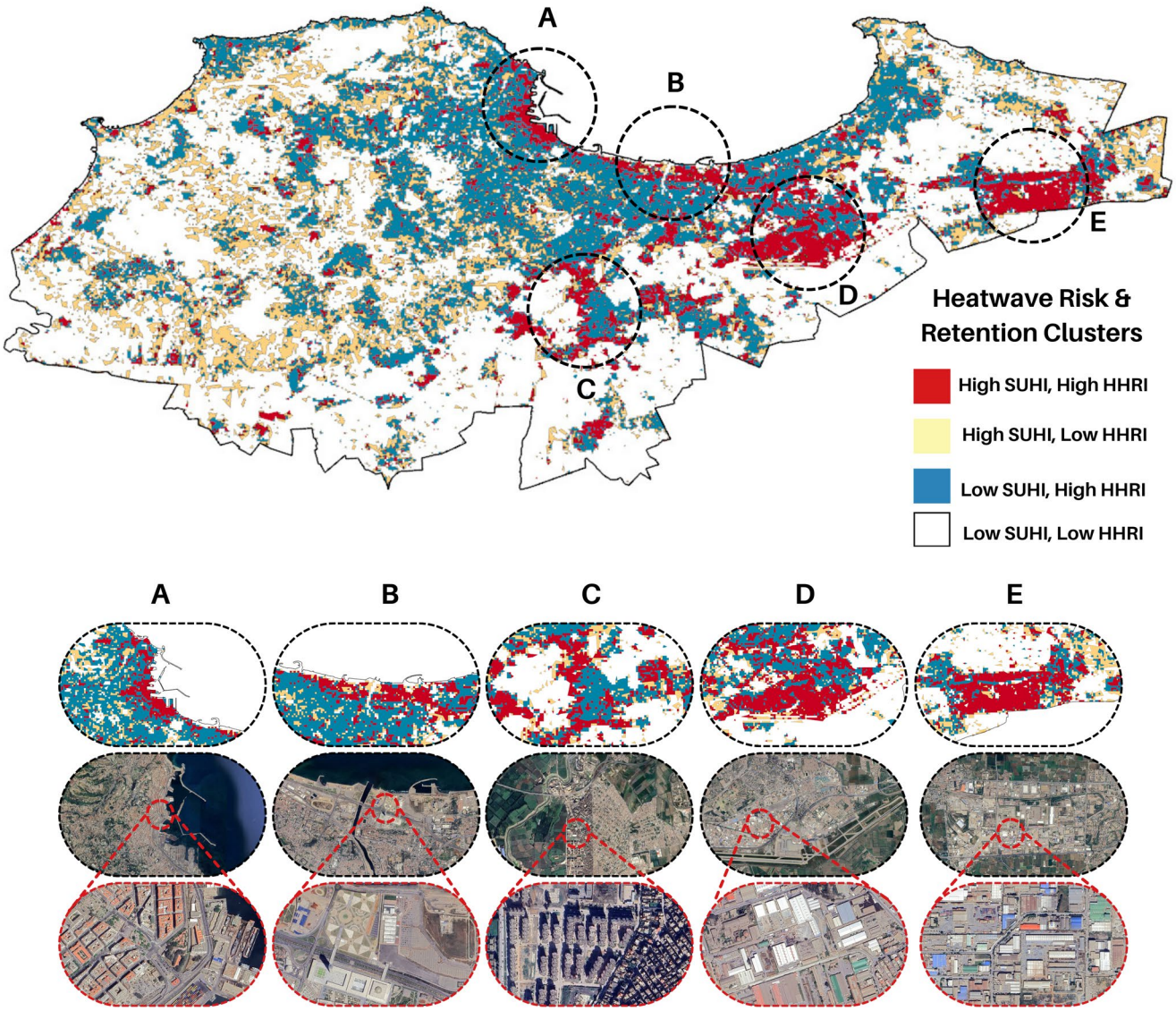

Fig. 7 Clustering of LCZs based on combined HHRI and SUHI values across Algiers. Insets (**A**–**E**) present detailed satellite views of critical zones

neighborhoods, such as Bir Khadem and Kouba, where population growth is more susceptible despite moderate thermal exposure. Cluster 4 (Low SUHI–Low HHRI) corresponds to areas with both low thermal intensity and low vulnerability, predominantly found in vegetated or low-density zones, including urban green spaces and forested areas, which act as natural moderators of heat and contribute to overall climate resilience.

4 Discussion

4.1 Key Findings and Recommendations

The distribution of HHRI across LCZs in Algiers reveals a strong link between urban morphology and heat-health vulnerability. These LCZ-based findings were built upon earlier research conducted at the municipal scale in Algiers (Zitouni et al. 2025), which first introduced the HHRI framework in the region. While that research identified patterns of HHR at a municipality level, the current analysis provides enhanced spatial resolution by linking HHRI directly to urban morphology.

LCZ 4 (Open High-rise) stands out as the most at-risk built type, with the highest share of zones classified as high or very high risk. This is likely driven by a mix of dense vertical development, limited vegetation, and high residential occupancy with varying adaptive capacities. Similar patterns were observed by Ma et al. (2023) and Yu et al. (2024), where high-rise areas with minimal ecological infrastructure correlated with elevated HHRI. LCZ 5 (Open Mid-rise) and LCZ 2 (Compact Mid-rise) also show considerable shares of elevated HHRI. Their moderate heights and open layouts often limit shading and increase exposure, which can contribute to heat stress when combined with population vulnerability. This pattern reflects the combined impact of urban morphology and socio-demographic factors, consistent with Su et al. (2024), who identified similar risks in comparable urban typologies. LCZ 8 (Large Low-rise) and LCZ 3 (Compact Low-rise) fall within the mid-risk range, reflecting moderate vulnerability.

While these zones retain heat, factors such as mixed land use or lower exposure levels may help mitigate overall risk. Moreover, LCZ 6 (Open Low-rise) and LCZ 1 (Compact High-rise) show lower HHRI among urban types. Despite thermal exposure, their relatively stronger infrastructure and reduced social vulnerability contribute to lower risk levels. In particular, LCZ 1 exhibited lower-than-expected HHRI values, which contrasts with many other studies where compact high-rise areas are often associated with elevated risk (Guo et al. 2025; Zhang et al. 2025; Zou et al. 2024). In Algiers, this anomaly is attributed to two factors: first, LCZ 1 is the least represented among the built-up classes; second, areas falling under this category tend to feature better infrastructure, organized green spaces, and improved shading conditions, which may help mitigate heat stress. These findings align with those of Xiang et al. (2024), who also noted the role of service access in offsetting vulnerability. Natural land cover types predominantly fall within low or very low HHRI categories, serving as ecological buffers that limit both heat accumulation and population exposure. Their consistent association with minimal risk underscores the value of integrating vegetated and open spaces into urban design, as highlighted by Yang et al. (2024) and Zhang et al. (2025). Overall, HHRI in Algiers exhibits a distinct spatial pattern, with the highest risks concentrated in open and mid-rise built forms. These insights are essential for guiding targeted adaptation measures in vulnerable zones and for preserving natural landscapes that contribute to urban thermal regulation.

This pattern is further supported by the SUHI intensity observed across the same LCZ classes, which aligns with findings from other Mediterranean and North African cities and reinforces the role of urban morphology in driving surface heat retention. LCZ 8 (Large Low-rise) recorded the highest SUHI intensity (3.83 °C), consistent with results from Oran, Algeria, where long-term urban expansion led to a sharp rise in surface temperatures (Soufiane et al. 2025). In Bari, Italy, similarly dense LCZs exhibited strong UHI effects, especially at night (Martinelli et al. 2020). Coastal breezes, however, helped mitigate heat in certain zones a feature also influencing parts of coastal Algiers.

Comparative studies in Central Europe, including Prague, Brno (Czech Republic), and Novi Sad (Serbia), reported peak SUHI values in compact and industrial LCZs during summer (Geletič et al. 2019), consistent with elevated thermal intensities found in LCZs 6 and 4 of Algiers. In East Asia, cities such as Wuhan and Hefei (China) also identified LCZ 8 as the most heat-intensive class (Shi et al. 2021; Xi et al. 2024), while high-resolution data from Beijing confirmed greater thermal loads in compact zones compared to open ones (Xia et al. 2022). Algiers reflected this contrast, with LCZs 6 and 8 showing greater heat accumulation compared to the relatively moderate intensities in LCZs 1 and 2. Together, these comparisons reinforce the broader conclusion: surface heat retention is highest in low-rise, dense, and unshaded forms, while compact and moderately vegetated zones offer only partial relief.

Although HHRI and SUHI individually offer valuable insights, they do not fully capture the spatial convergence of thermal exposure and population vulnerability. To address this, a clustering-based approach was applied to reveal compound risk typologies across Algiers, revealing distinct spatial patterns of heat-related risk in Algiers and offering

deeper insight into the overlap of thermal exposure and social vulnerability than single-variable analyses. Despite their potential, clustering approaches remain underutilized in heat risk research, such as vulnerability mapping in Taipei using PCA and LISA (Chen et al. 2022), model-based classification of social heat risk in Denver (Tuccillo and Buttenfield 2016), temperature–mortality clustering in China's Sichuan Basin (Wang et al. 2024a, b), and mortality hotspot detection in Paris (Benmarhnia et al. 2017), these approaches focused on either vulnerability or observed impacts. The article builds on this logic by jointly clustering SUHI and HHRI indicators, offering a comprehensive risk typology that supports forward-looking planning and intervention.

Cluster 1 represents the most critical risk zones, combining high SUHI and HHRI levels. These areas are concentrated in southern, eastern, and some coastal parts of Algiers, encompassing dense, poorly shaded urban forms primarily classified as LCZs 4, 6, and 8. They should be prioritized for adaptation measures, including urban greening, reflective materials, and community heat preparedness initiatives. Policy responses in these areas should be immediate and comprehensive, combining environmental and social strategies. Recommended actions include the implementation of heat action plans (Linares et al. 2020), deployment of cooling infrastructure such as shaded public spaces and shelters (Smail et al. 2024), and investment in nature-based solutions like green roofs (Arrar et al. 2024) and permeable surfaces (Ben Ratmia et al. 2024). In parallel, social resilience should be strengthened through improved access to healthcare and community-based climate awareness programs (Marí-Dell'Olmo et al. 2022).

Cluster 2 includes areas with high SUHI but low HHRI, indicating significant heat exposure but lower social vulnerability. In Algiers, these zones are often located in some coastal or central districts characterized by lower population density, commercial activity, or relatively high-income residential developments. Although these areas benefit from stronger infrastructure, better housing quality, and access to services, they still experience high levels of surface heat retention due to dense built-up areas and limited vegetation. To address thermal discomfort in these zones, planning responses should prioritize building-level retrofitting measures. This includes enhancing indoor thermal conditions through improved ventilation design tailored to Algiers' Mediterranean climate (Tellache et al. 2025), and adopting passive cooling strategies to reduce indoor heat buildup during summer peaks.

Cluster 3 includes socially vulnerable zones with lower SUHI values. Although these areas are not the hottest, they represent a significant concern due to their elevated HHRI levels. In Algiers, such zones are commonly found in aging neighborhoods, informal settlements, and peri-urban communities where infrastructure is weak and access to essential services is limited. These areas are home to populations with reduced adaptive capacity, such as the elderly, low-income households, and socially marginalized groups. While surface heat exposure is moderate, the underlying social vulnerability increases health risks during heat events. In this context, responses should prioritize social support systems and public health-based interventions, particularly those targeting elderly populations (Mahia et al. 2025).

Finally, Cluster 4 represents the most resilient areas, characterized by low heat exposure and low vulnerability. These zones are primarily located along the coast and in vegetated peri-urban areas of Algiers, where natural or compact urban forms support favorable microclimates. While they may not require immediate intervention, maintaining their thermal and social resilience should remain a planning priority. This includes enforcing land use regulations that protect vegetated and open spaces (Soares et al. 2021), preventing unplanned densification, and encouraging the replication of their design characteristics in future urban development (Erlwein and Pauleit 2021). Preserving these features will be essential to ensure long-term climate adaptability and urban health stability.

4.2 Strengths and Limitations

The primary contribution of this article lies in the use of unsupervised machine learning to jointly cluster SUHI intensity and HHRI, producing a typology of compounded heat risk across Algiers. As the first research to apply this integrated approach, it introduces a replicable method that merges thermal exposure and health vulnerability into a coherent spatial framework. The resulting hotspot typologies provide high spatial resolution, enabling the precise localization of risk zones and enhancing the capacity for place-specific adaptation planning.

In addition to this methodological advancement, the article presents the first long-term (2015–2023) assessment of SUHI patterns in Algiers, revealing how surface temperature varies across LCZs. This provides new spatial insights into surface heat retention across urban morphologies in the region. Furthermore, it represents only the second known application of HHRI in Algeria, and the first to examine its variation across LCZs, adding valuable knowledge to a region where heat-related health risk assessments remain scarce. The framework developed here is adaptable for use in other urban areas, particularly in data-limited regions. By combining remote sensing data, demographic indicators, and spatial analysis within a LCZ-based approach, the methodology supports replicability and comparative analysis across cities facing similar climate pressures.

However, the research has several limitations. The absence of high-resolution ground meteorological data limited the ability to estimate heatwave frequency with finer spatial accuracy. The lack of local health records restricted the direct validation of HHRI values against morbidity or mortality data. A limitation was also noted in previous heat-health risk studies (Wu et al. 2024; Wu, Zhao, Wu et al. 2024a, b; Zha et al. 2024). Moreover, key social and infrastructural variables, such as access to cooling and housing quality could not be included due to data constraints. These gaps, while not undermining the article's findings, point to areas for future enhancement to improve the precision and policy relevance of integrated heat risk models.

Altogether, this research lays the foundation for more spatially explicit and locally informed approaches to heat risk governance in Algiers and other climate-vulnerable Mediterranean cities.

4.3 Implications and Future Work

The clustering-based integration of SUHI and HHRI presented in this research offers a practical tool for advancing both public health preparedness and climate-resilient urban planning in Algiers and other Mediterranean cities. By distinguishing spatial typologies of heat-related risk, the analysis enables local health authorities to prioritize interventions in areas where vulnerable populations are most exposed. This supports more effective deployment of early heat warning systems, emergency medical preparedness, and community outreach, particularly for elderly populations and low-income neighborhoods.

For urban planners, the results highlight the importance of morphology-informed design strategies. High-risk clusters, often concentrated in dense, low-rise, or poorly shaded areas, targeted interventions such as vegetative retrofitting, reflective materials, and stricter land-use regulations that prevent further thermal intensification. Importantly, we also suggest that policymakers and planners initiate interventions not only in Cluster 1 areas but also urgently in Cluster 2 zones such as Mhelma and Sidi Abdellah. These newly urbanized districts are expected to absorb large population inflows in the coming years. Without the timely incorporation of adaptive measures, such as green and blue infrastructure, these zones risk shifting into Cluster 1 conditions, creating significant threats to public health and urban resilience. At the same time, areas identified as thermally and socially resilient should be preserved as cooling corridors or models for new urban development. The spatial typology can also support zoning policies that align building typologies with adaptation capacities.

In the Mediterranean context, where compact development, aging infrastructure, and climatic variability intensify heat-related risks, this integrative approach provides a replicable framework for guiding cross-sectoral action. Globally, the method can be scaled or adapted for use in other cities facing similar data constraints, helping to direct limited resources toward neighborhoods with the greatest compound risks.

Future work should expand this framework by integrating finer-scale datasets, such as access to healthcare facilities, urban vegetation indices, and building-level material characteristics. As this is the first study of its kind in North Africa, establishing a robust baseline for summer heat risk was a necessary starting point. Future studies will expand on this by exploring inter-annual variability and broader temporal dynamics. Additionally, linking cluster-based classifications with empirical health and mortality data would improve validation and policy relevance. Comparative applications in other climate-vulnerable urban regions could also help refine global typologies of HHR and inform more equitable adaptation strategies. From a methodological perspective, future studies should explore advanced machine learning algorithms, such as ensemble methods or deep learning, for LCZ classification and HHRI assessment (Table 4).

Table 4 Summary of urban heat risk clusters identified in Algiers

Type	SUHI	HHRI	Location Example	Description	Policy Implication
Cluster 1	High	High	Rouiba (Industrial zone) and Dar El Bida (Aeroport)	Critical hotspots with both high surface heat and high social vulnerability	Immediate intervention: urban greening, cooling infrastructure, and social support
Cluster 2	High	Low	Sidi Fredj (Coastal line) and Sidi Abdellah	Thermally intense areas with relatively low vulnerability	Building retrofits passive cooling strategies prevent future vulnerability
Cluster 3	Low	High	Kouba and Bir Khadem	Socially vulnerable areas with moderate heat exposure	Focus on public health services, heat awareness, and community preparedness
Cluster 4	Low	Low	Forests and Cultivated lands	Thermally and socially resilient areas, often vegetated or low-density zones	Preservation of green infrastructure and avoidance of future densification

5 Conclusion

This research presented a spatially integrated assessment of urban heat risk in Algiers by (1) quantifying SUHI intensity using satellite-derived LST data (2015–2023), (2) mapping HHRI across LCZs based on hazard, exposure, and vulnerability components, and (3) applying an unsupervised clustering approach to identify compounded risk typologies. The results revealed significant spatial disparities, with urban forms such as open high-rise, open low-rise, and large low-rises exhibiting elevated heat retention and social sensitivity. Clustering SUHI and HHRI values enabled the identification of four distinct typologies, including zones where thermal stress and vulnerability converge, offering actionable insights for targeted heat adaptation.

For planners and policymakers, these findings underscore the need for morphology-informed strategies, including urban greening, reflective materials, and improved public health access in high-risk areas. The methodology developed is universally replicable and provides an effective framework for identifying urban heat-health risk typologies. Future research should build on this approach by integrating health outcome data such as morbidity, emergency admissions, and mortality records to validate the risk typologies and strengthen the empirical foundation for heat resilience planning. Such integration will enhance model accuracy and support more targeted public health interventions.

Acknowledgements We would like to acknowledge the Sustainable Building Design Lab for providing access to data processing software and for their valuable assistance in data analysis and research coordination.

Author Contributions Dyna Chourouk Zitouni: Conceptualization, Data curation, Methodology, Software, Visualization, Writing – original draft, Writing – review & editing. Djihed Berkouk: Conceptualization, Supervision, Writing – review & editing. Mohamed Elhadi Matallah: Conceptualization, Supervision, Writing – review & editing. Mohamed Akram Eddine Ben Ratmia: Methodology, Software, Visualization. Ayyoob Sharifi: Writing – review & editing. Shady Attia: Conceptualization, Supervision, Writing – original draft, Writing – review & editing.

Funding The authors declare that no funds, grants, or other support were received during the preparation of this manuscript.

Data Availability The data supporting the findings of this research can be accessed at https://doi.org/10.7910/DVN/D9WGVN.

Declarations

Competing Interests The authors have no relevant financial or non-financial interests to disclose.

References

Arrar HF, Kaoula D, Santamouris M, Foufa-Abdessemed A, Emmanuel R, Matallah ME, Ahriz A, Attia S (2024) Coupling of different nature base solutions for pedestrian thermal comfort in a mediterranean climate. Build Environ 256:111480. https://doi.org/10.1016/j.buildenv.2024.111480

Baqa MF, Lu L, Guo H, Song X, Alavipanah SK, Nawaz-ul-Huda S, Li Q, Chen F (2025) Investigating heat-related health risks related to local climate zones using SDGSAT-1 high-resolution thermal infrared imagery in an arid megacity. Int J Appl Earth Obs Geoinf 136:104334. https://doi.org/10.1016/j.jag.2024.104334

Bechtel B, Alexander PJ, Böhner J, Ching J, Conrad O, Feddema J, Mills G, See L, Stewart I (2015) Mapping local climate zones for a worldwide database of the form and function of cities. ISPRS Int J Geo-Inf 4(1):199–219. https://doi.org/10.3390/ijgi4010199

Ben Ratmia FZ, Ahriz A, Santi G, Bouzaher S, Mahar WA, Ben Ratmia MAE, Matallah ME (2024) Street design strategies based on Spatial configurations and Building external envelopes in relation to outdoor thermal comfort in arid climates. Sustainability 16(1). https://doi.org/10.3390/su16010221

Ben Ratmia MAE, Fezzai S, Zitouni DC, Matallah ME, Bouzaher S, Ben Ratmia FZ, Ramírez-Guerrero G (2025) Identifying hotspots of urbanization and agricultural growth: A spatio-temporal analysis of land use dynamics in Tolga, Algeria (1994–2024). Arid Land Res Manage 1–23. https://doi.org/10.1080/15324982.2025.2523921

Benmakhlouf I, Benmessaoud H, Bengusmia dJamal, Elhag M (2024) Interaction assessment of air pollutants and environmental variables in Aures, Algeria. Arab J Geosci 17(8):233. https://doi.org/10.1007/s12517-024-12025-z

Benmarhnia T, Kihal-Talantikite W, Ragettli MS, Deguen S (2017) Small-area spatiotemporal analysis of heatwave impacts on elderly mortality in Paris: a cluster analysis approach. Sci Total Environ 592:288–294. https://doi.org/10.1016/j.scitotenv.2017.03.102

Berrang-Ford L, Sietsma AJ, Callaghan M, Minx JC, Scheelbeek PFD, Haddaway NR, Haines A, Dangour AD (2021) Systematic mapping of global research on climate and health: a machine learning review. Lancet Planet Health 5(8):e514–e525. https://doi.org/10.1016/S2542-5196(21)00179-0

Boudreault J, Ruf A, Campagna C, Chebana F (2024) Multi-region models built with machine and deep learning for predicting several heat-related health outcomes. Sustain Cities Soc 115:105785. https://doi.org/10.1016/j.scs.2024.105785

Chen T-L, Lin H, Chiu Y-H (2022) Heat vulnerability and extreme heat risk at the metropolitan scale: a case study of Taipei metropolitan area, Taiwan. Urban Clim 41:101054. https://doi.org/10.1016/j.uclim.2021.101054

Ching J, Mills G, Bechtel B, See L, Feddema J, Wang X, Ren C, Brousse O, Martilli A, Neophytou M (2018) WUDAPT: an urban weather, climate, and environmental modeling infrastructure for the anthropocene. Bull Am Meteorol Soc 99(9):1907–1924. https://doi.org/10.1175/BAMS-D-16-0236.1

Crichton D (1999) The risk triangle. Nat Disaster Manage 102(3):102–103

Demuzere M, Hankey S, Mills G, Zhang W, Lu T, Bechtel B (2020) Combining expert and crowd-sourced training data to map urban form and functions for the continental US. Sci Data 7(1):264

Demuzere M, Kittner J, Bechtel B (2021) LCZ generator: a web application to create local climate zone maps. Front Environ Sci 9:637455. https://doi.org/10.3389/fenvs.2021.637455

Deng X, Yu W, Shi J, Huang Y, Li D, He X, Zhou W, Xie Z (2024) Characteristics of surface urban heat islands in global cities of

different scales: trends and drivers. Sustain Cities Soc 107:105483. https://doi.org/10.1016/j.scs.2024.105483

Erlwein S, Pauleit S (2021) Trade-offs between urban green space and densification: balancing outdoor thermal comfort, mobility, and housing demand. Urban Plan 6(1):5–19. https://doi.org/10.17645/up.v6i1.3481

Ferreira LS, Duarte DHS (2019) Exploring the relationship between urban form, land surface temperature and vegetation indices in a subtropical megacity. Urban Clim 27:105–123

Geletič J, Lehnert M, Savić S, Milošević D (2019) Inter-/intra-zonal seasonal variability of the surface urban heat island based on local climate zones in three central European cities. Build Environ 156:21–32

Guo F, Fan G, Zhao J, Zhang H, Dong J, Ma H, Li N (2025) Urban heat health risk inequality and its drivers based on local climate zones: a case study of Qingdao, China. Build Environ 275:112827. https://doi.org/10.1016/j.buildenv.2025.112827

Hadji R, Taib H, Hamed Y, Yahiaoui S, Bedri K (2025) Morphometric and land use integration for erosion susceptibility assessment in the Ma labiod watershed, NE Algeria, using a compound prioritization framework. J Afr Earth Sc 232:105831. https://doi.org/10.1016/j.jafrearsci.2025.105831

Huang F, Jiang S, Zhan W, Bechtel B, Liu Z, Demuzere M, Huang Y, Xu Y, Ma L, Xia W (2023) Mapping local climate zones for cities: a large review. Remote Sens Environ 292:113573. https://doi.org/10.1016/j.rse.2023.113573

IPCC (2021) *Sixth Assessment Report*. https://www.ipcc.ch/assessment-report/ar6/

Li F, Yigitcanlar T, Nepal M, Nguyen K, Dur F (2023) Machine learning and remote sensing integration for leveraging urban sustainability: a review and framework. Sustain Cities Soc 96:104653. https://doi.org/10.1016/j.scs.2023.104653

Li F, Yigitcanlar T, Nepal M, Thanh KN, Dur F (2024) A novel urban heat vulnerability analysis: integrating machine learning and remote sensing for enhanced insights. Remote Sens 16(16):16. https://doi.org/10.3390/rs16163032

Li F, Yigitcanlar T, Nepal M, Nguyen K, Dur F, Li W (2025) Mapping heat vulnerability in Australian capital cities: a machine learning and multi-source data analysis. Sustain Cities Soc 119:106079. https://doi.org/10.1016/j.scs.2024.106079

Linares C, Díaz J, Negev M, Martínez GS, Debono R, Paz S (2020) Impacts of climate change on the public health of the Mediterranean basin population-current situation, projections, preparedness and adaptation. Environ Res 182:109107. https://doi.org/10.1016/j.envres.2019.109107

Liu H, Li M, Zhan Q, Ma Z, He B-J (2025) Homogeneity and heterogeneity of diurnal and nocturnal hotspots and the implications for synergetic mitigation in heat-resilient urban planning. Comput Environ Urban Syst 117:102241. https://doi.org/10.1016/j.compenvurbsys.2024.102241

Ma L, Huang G, Johnson BA, Chen Z, Li M, Yan Z, Zhan W, Lu H, He W, Lian D (2023) Investigating urban heat-related health risks based on local climate zones: a case study of Changzhou in China. Sustain Cities Soc 91:104402. https://doi.org/10.1016/j.scs.2023.104402

Mahia L, Berkouk D, Bouzir TAK, Pigliautile I, Pisello AL (2025) Investigating the relationship between Spatial Morphology, meteorological Factors, and elderly people responses in a traditional Algerian village. Sustainable Cities Soc 106212. https://doi.org/10.1016/j.scs.2025.106212

Marí-Dell'Olmo M, Oliveras L, Barón-Miras LE, Borrell C, Montalvo T, Ariza C, Ventayol I, Mercuriali L, Sheehan M, Gómez-Gutiérrez A (2022) Climate change and health in urban areas with a mediterranean climate: a conceptual framework with a social and climate justice approach. Int J Environ Res Public Health 19(19):12764. https://doi.org/10.3390/ijerph191912764

Martinelli A, Kolokotsa D-D, Fiorito F (2020) Urban heat island in Mediterranean coastal cities: the case of Bari (Italy). Climate 8(6):79

Matallah ME, Matzarakis A, Boulkaibet A, Ahriz A, Zitouni DC, Ratmia FZB, Mahar WA, Ghanemi F, Attia S (2025) Refining climate zoning in North africa: A 30-Year analysis of heating and cooling degree days for energy planning and adaptation. Energy Build 115852. https://doi.org/10.1016/j.enbuild.2025.115852

Rahmani N, Sharifi A (2024) Urban heat dynamics in local climate zones (LCZs): A systematic review. Build Environ 112225. https://doi.org/10.1016/j.buildenv.2024.112225

Shi L, Ling F, Foody GM, Yang Z, Liu X, Du Y (2021) Seasonal suhi analysis using local climate zone classification: a case study of Wuhan, China. Int J Environ Res Public Health 18(14):7242

Smail SA, Zemmouri N, Djenane M, Nikolopoulou M (2024) Investigating the transient conditions of Sabat space and its influence on pedestrian sensations during thermal walks. Algiers' casbah case study. Build Environ 111760. https://doi.org/10.1016/j.buildenv.2024.111760

Soares R, Corvacho H, Alves F (2021) Summer thermal conditions in outdoor public spaces: a case study in a mediterranean climate. Sustainability 13(10):5348. https://doi.org/10.3390/su13105348

Soufiane IM, Djaouad RD, Farah B, Djamel S (2025) Spatiotemporal impact of urbanization on urban heat island using Landsat imagery in Oran, Algeria: 1984–2024. Urban Sci. https://doi.org/10.3390/urbansci9040095

Stewart ID, Oke TR (2012) Local climate zones for urban temperature studies. Bull Am Meteorol Soc 93(12):1879–1900. https://doi.org/10.1175/BAMS-D-11-00019.1

Su R, Yang C, Xu Z, Luo T, Yang L (2024) Assessment of fine-scale urban heat health risk and its potential driving factors based on local climate zones in Shenzhen, China. ISPRS Int J Geo-Inf 13(10):367. https://doi.org/10.3390/ijgi13100367

Tellache A, Lazri Y, Laafer A, Attia S (2025) Development of a benchmark model for residential buildings with a mediterranean climate: the Aero-Habitat in Algiers City. Sustainability 17(3):831. https://doi.org/10.3390/su17030831

Tuccillo JV, Buttenfield BP (2016) Model-Based Clustering of Social Vulnerability to Urban Extreme Heat Events. In J. A. Miller, D. O'Sullivan, & N. Wiegand (Eds), *Geographic Information Science* (Vol. 9927, pp. 114–129). Springer International Publishing. https://doi.org/10.1007/978-3-319-45738-3_8

Verdonck M-L, Demuzere M, Hooyberghs H, Beck C, Cyrys J, Schneider A, Dewulf R, Van Coillie F (2018) The potential of local climate zones maps as a heat stress assessment tool, supported by simulated air temperature data. Landsc Urban Plann 178:183–197. https://doi.org/10.1016/j.landurbplan.2018.06.004

Wang J, Nikolaou N, Heiden ADM, Irrgang C (2024a) High-resolution modeling and projection of heat-related mortality in Germany under climate change. Commun Med 4(1):206. https://doi.org/10.1038/s43856-024-00643-3

Wang W, Zeng J, Li X, Liao F, Zhang T, Yin F, Deng Y, Ma Y (2024b) Using a novel strategy to identify the clustered regions of associations between short-term exposure to temperature and mortality and evaluate the inequality of heat-and cold-attributable burdens: a case study in the Sichuan Basin, China. J Environ Manage 349:119402. https://doi.org/10.1016/j.jenvman.2023.119402

WorldPop (2023) Global high-resolution population datasets (2000–2020) [Data set]. University of Southampton. https://doi.org/10.5258/SOTON/WP00646

Wu H, Xu Y, Zhang M, Su L, Wang Y, Zhu S (2024a) Spatially explicit assessment of the heat-related health risk in the Yangtze River Delta, China, using multisource remote sensing and socioeconomic data. Sustain Cities Soc 104:105300. https://doi.org/10.1016/j.scs.2024.105300

Wu H, Zhao C, Zhu Y, Pan Y (2024b) A multiscale examination of heat health risk inequality and its drivers in mega-urban agglomeration: a case study in the Yangtze river Delta, China. J Clean Prod 458:142528. https://doi.org/10.1016/j.jclepro.2024.142528

Xi Y, Wang S, Zou Y, Zhou X, Zhang Y (2024) Seasonal surface urban heat island analysis based on local climate zones. Ecol Indic 159:111669

Xia H, Chen Y, Song C, Li J, Quan J, Zhou G (2022) Analysis of surface urban heat Islands based on local climate zones via spatiotemporally enhanced land surface temperature. Remote Sens Environ 273:112972

Xiang Y, Yuan C, Cen Q, Huang C, Wu C, Teng M, Zhou Z (2024) Heat risk assessment and response to green infrastructure based on local climate zones. Build Environ 248:111040. https://doi.org/10.1016/j.buildenv.2023.111040

Yang L, Yang C, Zhou W, Chen X, Wang C, Liu L (2024) Mapping the spatial and seasonal details of heat health risks in different local climate zones: a case study of Shanghai, China. Remote Sens 16(18):3513. https://doi.org/10.3390/rs16183513

Ye J, Yang F (2025) Towards multi-scale and context-specific heat health risk assessment-a systematic review. Sustain Cities Soc 119:106102. https://doi.org/10.1016/j.scs.2024.106102

Yu W, Yang J, Sun D, Xue B, Sun W, Ren J, Yu H, Xiao X, Xia JC, Li X (2024) Shared insights for heat health risk adaptation in metropolitan areas of developing countries. IScience. https://doi.org/10.1016/j.isci.2024.109728

Zha F, Lu L, Wang R, Zhang S, Cao S, Baqa MF, Li Q, Chen F (2024) Understanding fine-scale heat health risks and the role of green infrastructure based on remote sensing and socioeconomic data in the megacity of Beijing, China. Ecol Ind 160:111847. https://doi.org/10.1016/j.ecolind.2024.111847

Zhang X, Zhu Y, Gan W, Zou Y, Wu Z (2024) Mapping heterogeneity: spatially explicit machine learning approaches for urban value uplift characterisation and prediction. Sustain Cities Soc 114:105742. https://doi.org/10.1016/j.scs.2024.105742

Zhang C, Yang Y, Yu L (2025) Assessing urban surface thermal environment and heat health risk in Chinese cities: a twenty-year study. Urban Clim 59:102304. https://doi.org/10.1016/j.uclim.2025.102304

Zhao Z, Sharifi A, Dong X, Shen L, He B-J (2021) Spatial variability and temporal heterogeneity of surface urban heat island patterns and the suitability of local climate zones for land surface temperature characterization. Remote Sens 13(21):4338. https://doi.org/10.3390/rs13214338

Zhou Y, Wan E (2025) Analysis of Beijing's cold and heat risks based on infectious disease trends. Sustain Cities Soc 119:106117. https://doi.org/10.1016/j.scs.2024.106117

Zhou D, Xiao J, Bonafoni S, Berger C, Deilami K, Zhou Y, Frolking S, Yao R, Qiao Z, Sobrino JA (2018) Satellite remote sensing of surface urban heat islands: progress, challenges, and perspectives. Remote Sens 11(1):48. https://doi.org/10.3390/rs11010048

Zhou X, Okaze T, Ren C, Cai M, Ishida Y, Watanabe H, Mochida A (2020) Evaluation of urban heat islands using local climate zones and the influence of sea-land breeze. Sustain Cities Soc 55:102060. https://doi.org/10.1016/j.scs.2020.102060

Zitouni DC, Berkouk D, Matallah ME, Attia S (2024) *Dataset for Heat Health Risk and Thermal Comfort Assessment in Algiers (2001–2023)* [Data set]. Harvard Dataverse. https://doi.org/10.7910/DVN/D9WGVN

Zitouni DC, Berkouk D, Matallah ME, Ben Ratmia MAE, Attia S (2025) Advancing heat health risk assessment: hotspot identification of heat stress and risk across municipalities in Algiers. Algeria Atmosphere 16(4):484. https://doi.org/10.3390/atmos16040484

Zou B, Fan C, Li J (2024) Quantifying the influence of different block types on the urban heat risk in High-Density cities. Buildings 14(7):7. https://doi.org/10.3390/buildings14072131